3rd National Congress on Physical Sciences, 29 Sep. – 2 Oct. 2016, Sofia
Section: Physics of Earth, Atmosphere and Space

Numerical Simulations for Stably Stratified Flow in Complex Terrain for MATERHORN Field Program

R. Dimitrova[1,2], **Z. Silver**[2], **T. Zsedrovits**[2,3], **H.J.S. Fernando**[2,4]

[1]Department of Meteorology and Geophysics, Faculty of Physics, St. Kliment Ohridski University of Sofia, 5 James Bourchier Blvd., BG-1164 Sofia, Bulgaria
[2]Department of Department of Civil and Environmental Engineering and Earth Sciences, University of Notre Dame, IN 46556, USA
[3]Faculty of Information Technology and Bionics, Pazmany Peter Catholic University, H-1444 Budapest, Hungary
[4]Department of Aerospace and Mechanical Engineering, University of Notre Dame, IN 46556, USA

Abstract. Orography presents a significant forcing to the flow, and varieties that incorporate slopes, valleys, canyons, escarpments, gorges and bluffs (also known as complex terrain) span different space-time scales contributing to innumerable phenomena that stymie the predictability of mountain weather. The Advanced Research version of the Weather Research and Forecasting (WRF) system was used to investigate the ability of a mesoscale atmospheric model to predict key atmospheric phenomena observed during the Mountain Terrain Atmospheric Modeling and Observations (MATERHORN) field program. The WRF simulations were run with a 0.5 km horizontal grid resolution for selected Intense Observations Periods (IOP), and the analysis was focused on periods with synoptically driven stably stratified atmospheric boundary layers. Special software were developed for the needs of this research, capable of determining any of the 3D WRF variables with the ability to calculate the energy budget, and pressure anomalies along the streamline. This software gives an exceptional opportunity to investigate different phenomena related to real complex terrain which includes, but is not limited to dividing streamline height and flow separation, trapped lee waves, and vortex formation. Different conditions were evaluated to investigate flow patterns and characteristics to further understanding of physics based fundamental relationships for complex-terrain processes.

1 Introduction

The most complicated and extremely diverse pattern of atmospheric boundary-layer processes of complex terrain occur in response to multiplicity of forcing factors, acting primarily at the mesoscale and microscale. During quiescent conditions the local terrain and land-use

inhomogeneity induce thermally driven circulation, but when synoptic systems dominate, the local terrain characteristics will significantly modify the large-scale flow [1]. Both the mesoscale and microscale atmospheric motion become important in studying the diverse processes present in complex terrain. The two different scales of motion, and their interactions make the study of these processes extremely challenging.

Many of the existing theories use uniform, unidirectional velocity and constant buoyancy frequency, which is not appreciable for the real flow [2-13]. The main assumption of linear theory is that velocity perturbations are less significant than the undisturbed mean flow velocity, another questionable assumption for real flow conditions. A lot of experimental studies and theories have concentrated on 2D or 3D flow over the surface of axisymmetric obstacle. Obviously, three dimensional shapes have much more governing parameters than the two-dimensional case, and non-axisymmetric obstacles increases the difficulty of understanding and presentation of flow patterns because of the directional sensitivity. The slope angle, ground roughness and slope smoothness are a few of the parameters that are not taken into account in the known theories and inhomogeneity of flow and topography ahead of the obstacle is an additional complicating factor.

This study investigates 3D flow that overran and around a non-symmetric and rugged obstacle. The flow-terrain interaction induced additional disturbances in the field that spread out laterally as well as vertically. The known theories are too limited for direct use in our study. Due to this reason, a numerical approach was applied in this work. Modelling allows for a broader understanding of the physical processes and mechanisms involved. A combination of numerical simulations over real topography and evaluation of model performance using observations can be a powerful method to provide greater insight on synoptic flow modification by mountainous terrain.

2 Experimental Set Up

The Weather Research and Forecasting (WRF) model (`http://www2.mmm.ucar.edu/wrf/users/`) was employed for these simulations. Some modifications were made in the distributed version. The updated database (land-cover and terrain elevation) together with a new parametrization for soil thermal conductivity in the NOAA land-surface model for silt loam and sandy loam soils was used. The latter modification was proposed by [14], which was found to reduce the nocturnal temperature bias significantly. No data assimilation was applied in our study, in contrast to [14]. Numerical simulations with the same domain have been conducted in previous work related to Mountain Terrain Atmo-

spheric Modelling and Observations (MATERHORN) field program [15], and the best model configuration was selected.

2.1 Domain of simulations

The modelling domain was centred at 113°W, 40°N, using a Lambert Projection. The fine-scale horizontal resolution for the inner domain was accomplished by using four domains, nesting 32 km, 8 km, 2 km, and 0.5 km. Fifty terrain-following vertical (eta) levels were selected with a greater number of levels below 1 km (26 levels), and with 21 of these located below 0.5 km above the surface. The location of the model domains with an enlarged view of the fourth domain with 0.5 km horizontal grid, are shown in Figure 1a. The isolated obstacle Granite Peak (with elevation of 2158 m) was of special interest in this study. The various surface and vertically profiling instruments on site operated during Intense Observation Periods (IOPs) have been depicted on the map in Figure 1b. Data recorded by these instruments have been used for model validation.

The NCEP Final Operational Model Global Tropospheric Analyses dataset (`http://rda.ucar.edu/datasets/ds083.2/`) was utilized to establish the initial and boundary conditions for the WRF simulations of this work. This dataset provides the initial and boundary conditions for the largest model domain (32 km) at every six hour period (00, 06, 12, 18 UTC).

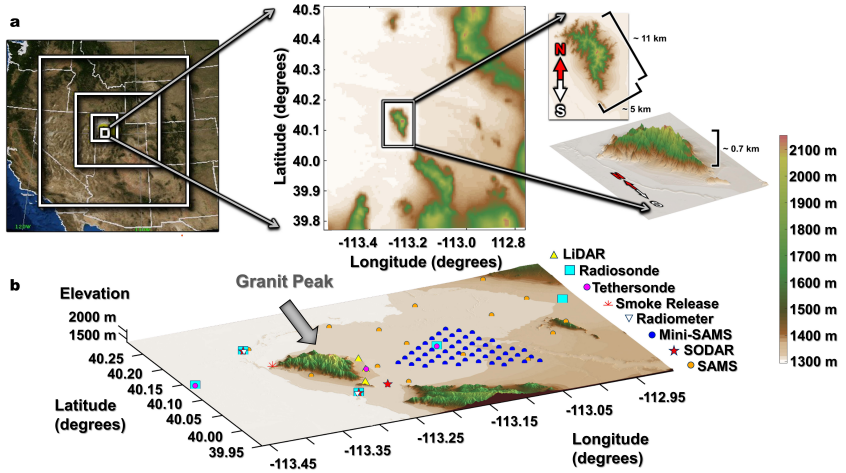

Figure 1: WRF domain configuration: (a) 4 domains with 32 km, 8 km, 2 km, and 0.5 km grids; (b) topography with instruments set-up around Granite Peak used for model validation.

2.2 Periods of simulations

This work was focused on selecting IOPs that coincided with synoptic conditions, observed during the MATERHORN program. An IOP was defined as quiescent (< 5 m/s), moderate (between 5–10 m/s) or synoptically driven (> 10 m/s) based on wind speed at the 700 mb level [16]. For our purposes, it was important to select periods where local flow conditions were dominated by synoptic weather patterns. Model results were saved in the output file for every 20-minute interval with a minimum model spin-up time of 12 hours in advance of each IOP case. Only hours with stable conditions have been selected and two examples are presented in this study.

2.3 Model options

The WRF model physical parametrizations include the following: microphysical scheme [17], the rapid radiative transfer model longwave radiation parametrization [18], the Dudhia shortwave radiation parametrization [19] and the Noah land-surface model [20]. Cumulus physics was parameterized only for the two outer most domains (32 km and 8 km grids). The parameterization scheme selected for this was the Simplified Arakawa-Schubert. Finally, the Planetary Boundary Layer parameterization was selected based on previous comparative model validation studies [15]. The Quasi-Normal Scale Elimination (QNSE) [21] performed the best for stable conditions, which was employed in this study.

3 Developing of New Tool for Visualization and Analysis

In order to perform this study, a new tool needed to be developed in order to trace a single or multiple 3D streamlines throughout the model domain to be able to perform an analysis over the streamlines. The program uses the MatLab environment and this tool is capable of deriving quantities that include: kinetic and potential energy, pressure perturbations, buoyancy frequency. In addition dimensionless parameters related to dividing streamline theory that describes the nonlinear flow features are computed along a given streamline. All variables are interpolated along the line following the velocity vector.

The 3D vector is computed for the starting point by a sequence of interpolations with linear local Lagrange basis functions (Figure 2a). Both the linear and cubic systems were evaluated using a 3D sine wave field. Although the cubic interpolation produced more accurate result in general, the tests confirmed that a cubic interpolation was inaccurate for use with the 500 m model grid spacing close to the ground. The cubic interpo-

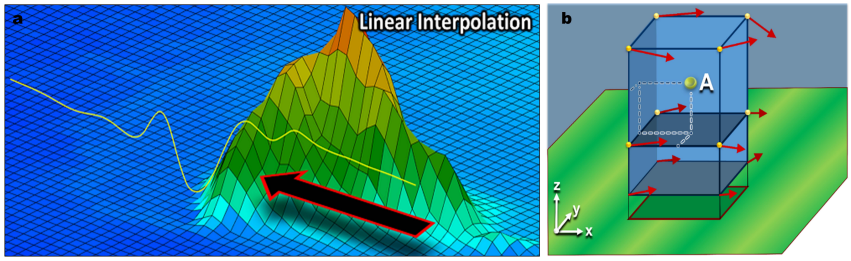

Figure 2: Path tracing methodology: (a) visualization of the path; (b) the point specified inside of eight grid volume centers.

lation does not provide an appropriate representation notwithstabding that it apperrs to resolve flow distortions that are an order of magnitude smaller than the grid resolution. Computing the tangent path taken by a passive scalar released in the WRF domain begins with the user specifying a starting point within the domain inside of eight grid volume centers as shown in Figure 2b. Each of the three wind vector components are interpolated as a separate function call. Specifying the scalar values of potential temeperature, presure, mixing ratio, and TKE at the nodes for subsequent function calls allows for the interpolation of each scalar to point A.

4 Model Verification

Although the domain and simulation settings were verified in the work [15], the simulations of this work were further verified using a similar methodology. Comparison charts of wind vectors at 10 m were generated

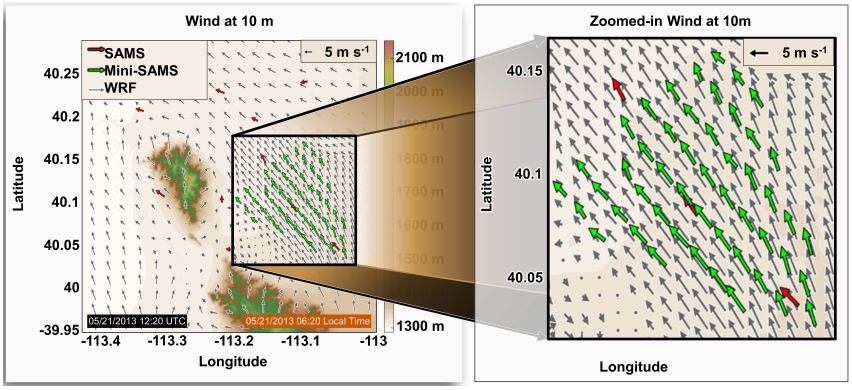

Figure 3: Wind vector comparison between model (grey) and observations (red and green) for 21st of May 2013, 12:20 UTC (06:20 local time).

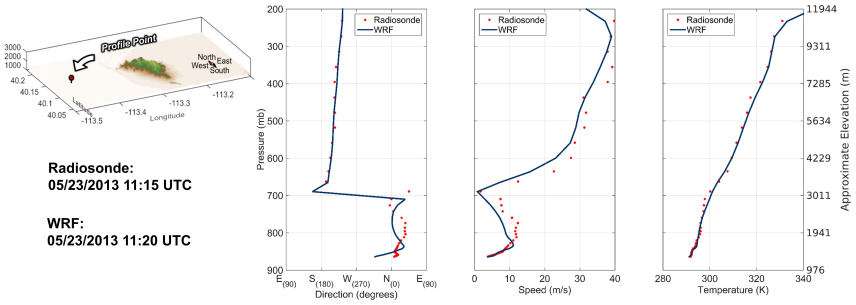

Figure 4: Vertical profiles of horizontal wind direction, wind speed, and temperature from the WRF model (blue line) and observations (red dots) for the selected period.

for each of the 20-minute output intervals in the model data, during the selected time window (7 pm – 11 am). Results from a selected case are shown in Figure 3. WRF model captures very well the nocturnal valley flow coming from the high mountain range located southeastern to the Granite Peak.

Profiles of potential temperature, horizontal wind speed and wind direction have been extracted from the WRF model data and compared with radiosonde releases from the point located at Playa salt field, west of Granite Peak (Figure 4). The model in general is able to capture the wind speed, wind direction, and temperature at various heights throughout the boundary layer and beyond. One of the cases that was investigated in detail in this study is described. This case is unique because a sharp change in wind direction at about 3000 m elevation produces a natural internal top boundary for the flow. Observed profiles for the velocity and temperature show that the model performs very well at capturing the vertical stretch of this exceptional phenomenon.

5 Results and Discussion

Various features related to terrain complexity will be discussed in this section. The main focus is the study of flow behaviour under different flow regimes and related phenomena that include: flow separation, trapped lee waves, vortices and rotors embedded in mountain waves that formed aloft above the downslope jet. The expansive variety of meteorological conditions that occurred in real atmosphere have made the task of selecting study cases very challenging. Two events with an approximately consistent predominant wind direction (approaching flow from an area characterized by flat terrain) and horizontal flow homogeneity away from the Granite Peak are presented. The location of the verti-

cal profile characterizing the upstream undisturbed flow are different for both presented cases depending on the flow direction. The dimensionless parameter Nh/U (where N is the buoyancy frequency; h – the height of the obstacle; U – the undisturbed mean velocity) are used for describing different cases. Mean Nh/U numbers are calculated using a representative average value of the mean approaching flow velocity from the modelled profile $U(x, y, z)$, and the buoyancy frequency of the entire layer. A small value of Nh/U ($Nh/U \ll 1$) implies that the effect of topography on the flow may be described as a linear perturbation, and nonlinear effects become more significant as Nh/U ($Nh/U \gg 1$) increases.

The description of both regimes of the approaching large scale flow is shown in Table 1 for two different values of the layer depth for each case. Flow properties for the selected cases are described in the next subsections. The differences between them depend on the value of Nh/U, but also on the details of the density structure at levels below mountain top height.

Table 1: Different flow regimes depending on Nh/U number

Case number	*Nh/U*	*Wind direction*	*Depth the layer [m]*	*Averaged wind speed [ms^{-1}]*	*Buoyancy frequency [s^{-1}]*
Case 1. Lee waves *25 May 2013* *13:20 UTC (7:20 local)*	3.23 2.38	S-SW S-SW	700 3700	8.1 9.8	0.035 0.032
Case 2. Hydraulic jump *23 May 2013* *10:20 UTC (4:20 local)*	2.27 1.89	N S	700 3700	10.5 12.6	0.033 0.033

5.1 Case 1 - lee waves; $Nh/U \sim 3$

Wave motions are oscillations in the field variables (such as velocity and pressure) that propagate in space and time. One example of trapped lee waves triggered by synoptic flow (~ 10 m/s) passing over an obstacle of finite length (Granite Peak) is shown in Figure 5. The approaching flow is composed of variable layers (Figure 5a) – a low level Southeasterly nocturnal jet due to local valley circulation, with a maximum velocity of approximately 6–7 m/s, and a Southwesterly synoptic flow above, with a maximum velocity at the hill top of approximately 10 m/s. Another stable layer with flow acceleration is present just above the mountain top. The horizontal temperature field and velocity streamlines at 3000 m elevation are shown (Figure 5b). The plot shows flow homogeneity away from the obstacle in the velocity field, but the temperature approaching flow is affected from the downslope flow formed from the mountain range south of the obstacle.

The isotherms of the potential temperature (Figure 5c) and streamlines in the cross-section (Figure 5d) clearly indicate lee wave formation lee-

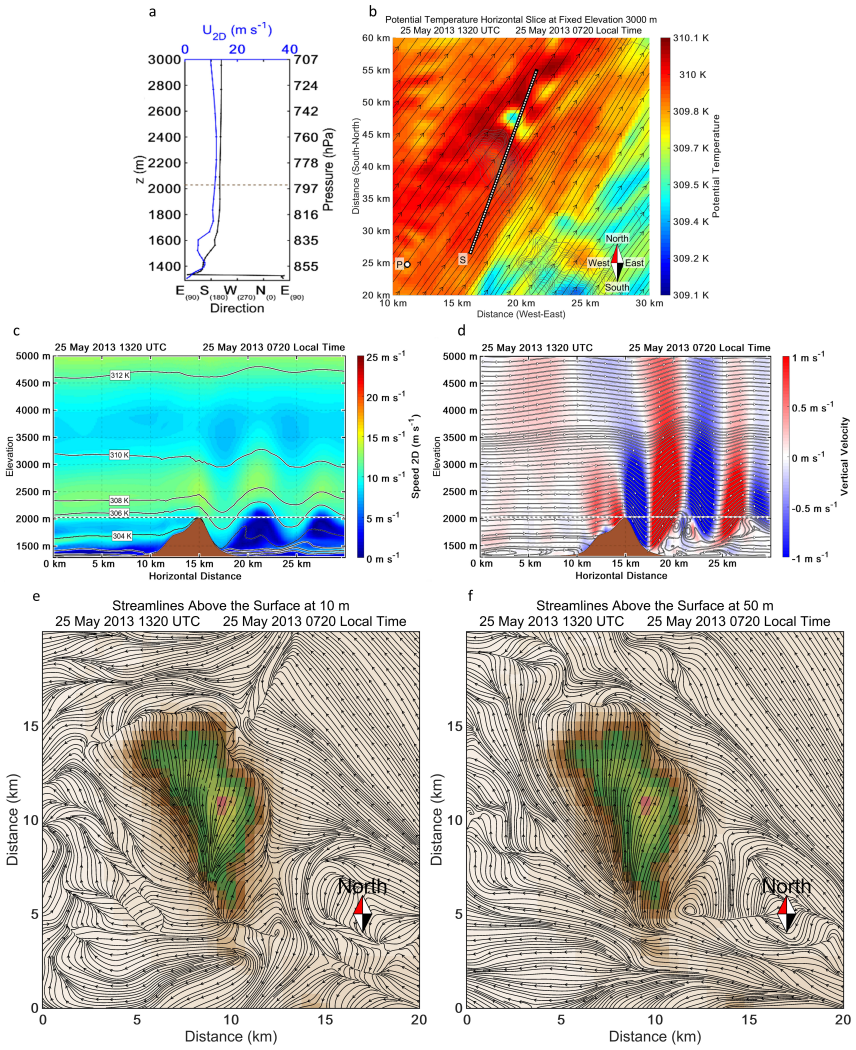

Figure 5: Flow field for the lee waves: (a) vertical profiles of wind speed and direction; (b) horizontal potential temperature and velocity streamlines at 3000 m elevation; (c) vertical cross-section of the velocity speed and potential temperature isotherms; (d) vertical slice of vertical velocity and parallel to the slice horizontal velocity with velocity streamlines; horizontal streamlines at 10 m (e) and 50 m (f) elevation.

ward of Granite Peak. The vertical velocity field shows the ascending and descending of the flow with a value of zero vertical velocity in the crests and troughs of the trapped wave. A region of high-speed 'shooting flow'

is located just above the mountain peak level windward. Over the lee slope it terminates in a series of large-amplitude lee waves with flow acceleration at the waves crest, with deceleration below. This leads to separation and the formation of vortices beneath the lee-wave crests (Figure 5d). The maximum upward displacement occurs not at the hill top, but at about 5–6 km downstream from the mountain top, after which the disturbance amplitude decays with height. Stronger shear downstream leads to formation of a rotor comprised of trapped lee waves. The flow over pass the obstacle in the horizontal streamlines at 10 m (Figure 5e). The horizontal disturbances due to local roughness elements leads to formation of more complicated patterns close to the ground. At 50 m above ground level, the flow field passing around the obstacle is smother, but is very different from the patterns observed in both laboratory and numerical experiments for an obstacle with a regular shape (Figure 5f).

5.2 Case 2 - hydraulic jump; $Nh/U \sim 2$

Strong downslope wind events are usually associated with strong cross-barrier flow, waves breaking aloft, and an inversion near the barrier top. Mountain waves are a different phenomenon to the mechanical turbulence produced in the lee of mountain ranges, and can exist as a smooth undulating airflow or may contain breaking waves and rotors. These features are also believed to be an important mechanism for transporting energy and momentum into the middle atmosphere, and are often associated with the formation of clear air turbulence. The low-level turbulent zone is another region of potentially significant turbulence. This region exists immediately downstream of the jump region and under a wave crest. Rotor axes typically occur at an altitude equal to or below the mountain-top peak, and in our case the rotors occurred at about half the height of Granite Peak and about 1 km downstream from the slope. In Ref. [22] found that along with resembling a hydraulic jump, a mountain-wave/rotor type is more likely to form when a strong near-mountain top inversion is present.

In the investigated Case 2, the capped inversion (Figure 6a) is strengthened by the reverse in the flow direction that occurs at approximately the hill height above the top, which prohibits the transfer of heat or matter through the internal boundary, as shown in Figures 6c, d. Three layers with different characteristics exist: a strong radiation inversion layer with a lower nocturnal jet; a stable layer with a smaller gradient and speed deceleration, and finally a reverse in flow direction and velocity acceleration to 30 m/s (Figure 6a). The reverse from Northerly to Southerly flow within a thin layer (thickness less than 500 m) forms a region with strong wind shear about 3000 m (Figure 6d). Flow acceler-

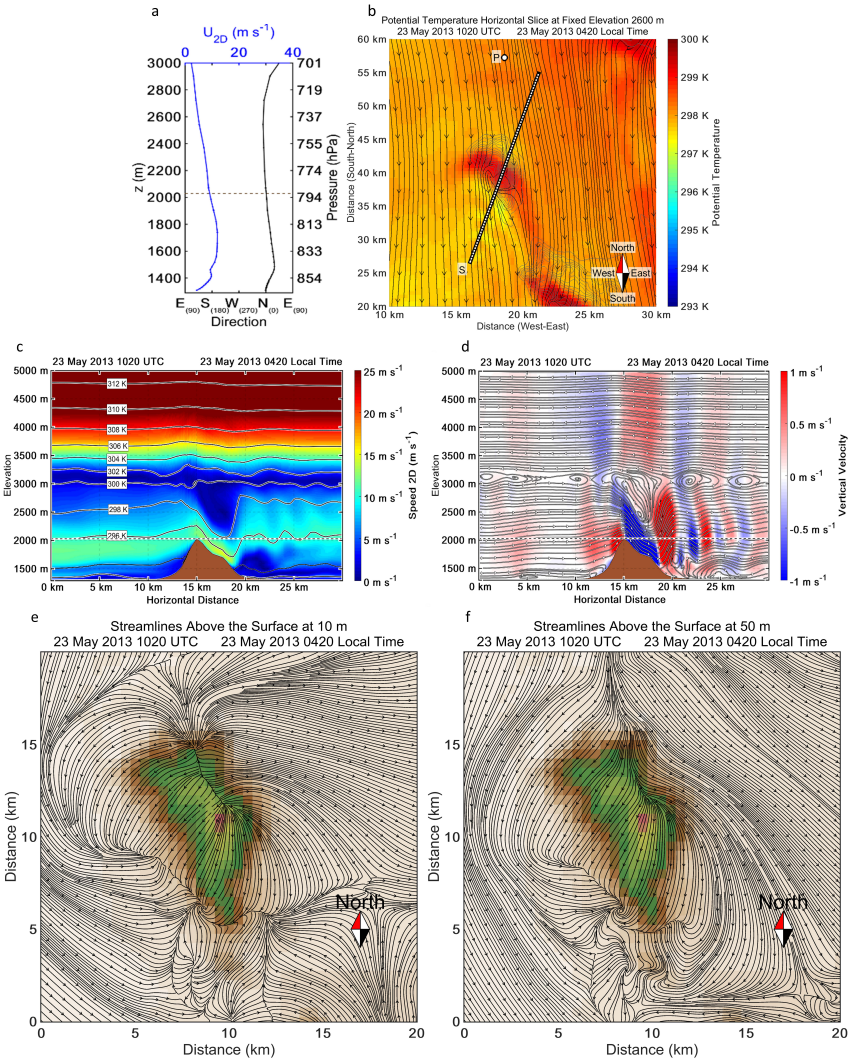

Figure 6: Flow field for the hydraulic jump: (a) vertical profiles of wind speed and direction; (b) horizontal potential temperature and velocity streamlines at 2600 m elevation; (c) vertical cross-section of the velocity speed and potential temperature isotherms; (d) vertical slice of vertical velocity and parallel to the slice horizontal velocity with velocity streamlines; horizontal streamlines at 10 m (e) and 50 m (f) elevation.

ation over the leeward slope in conjunction with a deep propagation in isotherms of the potential temperature is found to be in agreement with

observed phenomena within the Sierra Wave Experiment [23]. A horizontal cross-section showing streamlines at 10 m above ground level illustrates a different pattern to Case 1, with a strong return flow in the windward area. Due to the asymmetry of the hill and the gap flow south of the obstacle within the wake, the flow pattern is very complicated and horizontal vortices, typical for a symmetric obstacle are not present.

6 Conclusions

Investigation of 3D flow that overran and around a non-symmetric and rugged obstacle is very complicated as the flow-terrain interaction induced additional disturbances in the field that spread out laterally as well as vertically. The inhomogeneity of the flow, different shape based on the direction of the approaching flow, slope angle, ground roughness and slope smoothness, are a few of the parameters that are not taken into account in the known theories. The flow pattern related to real obstacle is very different from well-known fields discovered with laboratory and numerical experiments on regular axisymmetric shapes. Sometimes the main characteristic of the flow from these studies such as the upstream stagnation and separation points, or the presence of a lee-side separation region and associated wake, are not present in the real case. The height of the inversion layer related to the top of the obstacle and the nocturnal jet play a significant role on the flow pattern. The horizontal disturbances due to local roughness elements and jagged slopes provokes lateral and vertical eddy formation and makes the flow pattern incomparable with the known structure for idealized obstacles from theory and laboratory experiments. A specially developed code provides the unique opportunity to calculate the energy balance, pressure perturbations, and buoyancy frequency at each point over the streamline for natural 3D flow for realistic non-axisymmetric obstacles.

Acknowledgments

This research was funded by the US Office of Naval Research Award # N00014-11-1-0706, Mountain Terrain Atmospheric Modelling and Observations (MATERHORN) Program.

References

[1] Bodine D, Klein PM, Arms SC, Shapiro A (2009) Variability of surface air temperature over gently sloped terrain. J of Appl Meteorol and Climatol, 48(6):1117-1141

[2] Sheppard PA (1956) Airflow over mountains. Q J R Meteorol Soc 82(354):528-529

[3] Brighton PWM (1978) Strongly stratified flow past three-dimensional obstacles. Q J R Meteorol Soc 104(440):289-307
[4] Hunt JCR, Snyder WH (1980) Experiments on stably and neutrally stratified flow over a model three-dimensional hill. J Fluid Mech 96(04):671-704
[5] Smith RB (1989) Mountain-induced stagnation points in hydrostatic flow. Tellus 41A(3):270-274
[6] Lin Q, Lindberg WR, Boyer DL, Fernando HJS (1992) Stratified flow past a sphere. J Fluid Mech 240:315-354
[7] Sha W, Nakabayashi K, Ueda H (1998) Numerical study on flow pass of a three-dimensional obstacle under a strong stratification condition. J App Meteorol 37(10): 1047-1054
[8] Vosper SB, Castro IP, Snyder WH, Mobbs SD (1999) Experimental studies of strongly stratified flow past three-dimensional orography. J Fluid Mech 390:223-249
[9] Hunt JCR, Vilenski GG, Johnson ER (2006) Stratified separated flow around a mountain with an inversion layer below the mountain top. J Fluid Mech 556:105-119
[10] Ding L, Calhoun RJ, Street RL (2003) Numerical simulation of strongly stratified flow over a three-dimensional hill. Boundary-layer meteorol 107(1):81-114
[11] Li D, Calhoun RJ, Street RL (2002) Numerical simulation of strongly stratified flow over a three-dimensional hill. Boundary-Layer Meteorol 107:81-114
[12] Lindeman J, Broutman D, Eckermann SD, Ma J, Rottman J, Boybeyi Z (2012) Mesoscale model initialization of the Fourier method for mountain waves. J Atmos Sci 65:2749–2756
[13] Leo LS, Thompson MY, Di Sabatino S, Fernando HJS (2016) Stratified flow past a hill: dividing streamline concept revisited. Boundary-Layer Meteorol 159(3): 611–634
[14] Massey J, Steenburgh WJ, Hoch SW, Knievel JC (2014) Sensitivity of near-surface temperature forecasts to soil properties over a sparsely vegetated dryland region. J Appl Meteorol Clim 53(8): 1976-1995
[15] Dimitrova R, Silver Z, Zsedrovits T, Hocut CM, Leo LS, Di Sabatino S, Fernando HJS (2016) Assessment of planetary boundary-layer schemes in the Weather Research and Forecasting Mesoscale Model using MATERHORN field data. Boundary-Layer Meteorol 159(3):589–609
[16] Fernando HJS, Pardyjak ER, Di Sabatino S…Zsedrovits T. (2015) The MATERHORN: unraveling the intricacies of mountain weather. Bull Amer Meteor Soc 96(11):1945-1967
[17] Lin YL, Farley RD, Orville HD (1983) Bulk parametrization of the snow field in a cloud model. J Appl Meteorol 13(1):54-61
[18] Mlawer EJ, Taubman SJ, Brown PD, Iacono MJ, Clough SA (1967) Radiative transfer for inhomogeneous atmospheres: RRTM, a validated correlated-k model for the longwave. J Geophys Res Atmos 102(14): 16663-16682
[19] Dudhia J (1989) Numerical study of convection observed during the winter monsoon experiment using a mesoscale two-dimensional model. J Atmos Sci 46:3077–3107

[20] Chen F and Dudhia J (2001) Coupling an advanced land surface-hydrology model with the Penn State-NCAR MM5 modelling system. Part I: Model implementation and sensitivity. Mon Weather Rev 129(4):569-585

[21] Sukoriansky S, Galperin B, Perov V (2005) Application of a new spectral theory of stably stratified turbulence to the atmospheric boundary layer over sea ice. Boundary-Layer Meteorol 117(2):231-257

[22] Hertenstein R F and Kuettner JP (2005) Rotor types associated with steep lee topography: influence of the wind profile. Tellus 57(2):117-135

[23] Lester PF and Fingerhut WA (1974) Lower turbulent zones associated with mountain lee waves. Journal of Applied Meteorology 13(1):54-61